Intensified Eu(III)extraction using ionic liquids in small channels

Qi Li, Panagiota Angeli*

Department of Chemical Engineering, University College London, Torrington Place, London WC1E 7JE, UK

*Corresponding author: Tel.: ++44 (0) 20 7679 3832; Fax: ++44 (0)20 7383 2348; Email: p.angeli@ucl.ac.uk

Abstract

The extraction of Eu(III) from nitric acid solutions was studied in intensified small scale separation units using an ionic liquid solution (0.2M n-octyl(phenyl)-N,N-diisobutylcarbamoylmethyphosphine oxide (CMPO) -1.2M Tributylphosphate) (TBP)/1-butyl-3-methylimidazolium bis[(trifluoromethyl)sulfonyl]amide; ($[C_4min][NTf_2]$)as the extraction phase. The investigations were carried out in channels with 0.2 mm and 0.5 mm diameter for phase flowrates that result in plug flow with the aqueous solution as the dispersed phase. The interfacial area in plug flow and the velocity profiles within the plugs were studied with high speed imaging and bright field micro Particle Image Velocimetry. Distribution and mass transfer coefficients were found to have maximum values at nitric acid concentration of 1M. Mass transfer coefficients were higher in the small channel, where recirculation within the plugs and interfacial area are large, compared to the large channel for the same mixture velocities and phase flow rates. Within the same channel, mass transfer coefficients decreased with increasing residence time indicating that significant mass transfer takes place at the channel inlet where the two phases come into contact. The experimental results were compared with previous correlations on mass transfer coefficients in plug flows.

1. Introduction

Within the frame of process intensification, the miniaturization of chemical operations opens up new possibilities in separations. Microchemical systems with well-defined channel structures in the range of a few hundred μm are characterised by thin fluid layers and large surface-to-volume ratios, which improve heat and mass transfer rates, and, coupled with narrow residence time distributions, result in better process efficiency and control (Löwe and Ehrfeld, 1999; Kiwi-Minsker and Renken, 2005). The increased importance of interfacial phenomena, large interfacial areas and the ability to influence flow patterns make two-phase flows in small units particularly appealing. The benefits of microchannel operation have been clearly demonstrated for liquid-liquid extractions which often involve organic solvents with high hazard ratings (Kashid et al., 2005; Dessimoz et al., 2008; Kashid et al., 2010;

1

Assmann et al., 2013; Xu et al., 2013; Yang et al., 2013).As extraction efficiencies depend on concentration gradients, interfacial area and residence times (Okubo et al., 2008), the exact flow pattern within the separation unit becomes important. Plug (or segmented) flow in particular, where one phase forms dispersed plugs with diameter larger than the channel size separated by continuous phase slugs, is a preferred pattern because the circulation patterns forming in the two phases and the thin films separating the plugs from the channel wall enhance mass transfer (Burns and Ramshaw, 2001; Kashid et al., 2005; Okubo et al., 2008; Jovanović et al., 2012). In addition, the dispersed plug sizes are very regular and can be controlled via the choice of the inlet geometry which further reduces non-uniformities, common in large scale extraction units such as mixers-settlers(Khakpay et al., 2009). Knowledge of the interfacial area is very important in the understanding and modelling of extraction operations. Chemical reactions, e.g. alkaline hydrolysis of esters, have been used to obtain global values of interfacial area in units such as agitated contactors(Fernandes and Sharma, 1967), packed columns(Puranik and Sharma, 1970; Verma and Sharma, 1975)and two-impinging-stream reactors(Dehkordi, 2002).In small channels, where flow patterns are well defined, high speed imaging can be used to acquire details of the flow pattern locally, such as film thickness and plug length, and estimate the interfacial area (Ghaini et al., 2010; Xu et al., 2013).

One of the separations that can benefit from operation in small channels is the extraction of lanthanides from acidic solutions. Lanthanides with their strong photoluminescence and magnetic properties are important to many industrial applications. Europium and yttrium oxides can be used as fluorescing agents for anodic rays in television and monitor screens (Lee and Yang, 1995). Lanthanide oxides are used to colour ceramics and glasses (Goonan, 2011). Some compounds of lanthanides find applications as catalysts; for example oxides of thorium and cerium are used in the conversion of crude oil into common consumer products (Lew, 2010). Lanthanides have also been used to regulate nuclear reactors as control rods because they absorb neutrons (Kučera et al., 2007) and to make strong permanent magnets (Wang et al., 2011). Scarcity on natural resources means that the large quantities of lanthanides present in electronic waste such as spent fluorescent lamps (Rabah, 2008), computer monitor scraps (Resende and Morais, 2010) and colour TV tubes (De Morais, 2000), need to be recycled. In the field of spent nuclear fuel reprocessing, recovery of the trivalent actinides and lanthanides is a key step in high-level waste management. Since trivalent lanthanides cannot be extracted by TBP, they are rejected to high-level liquid waste in the PUREX process (Rout et al., 2011a). They can, however, be extracted by the TRUEX solvent, which is a mixture of 0.2 M CMOP- 1.2 M TBP in n-dodecane (Horwitz et al., 1982; Schulz and Horwitz, 1986).

Further intensification of the extraction process can be achieved by using room temperature ionic liquids (RTILs or ILs), which have emerged as alternatives to organic solvents for catalytic reactions and separations. Ionic liquids are salts with very low vapour pressure that can dissolve a wide range of organic and inorganic compounds. It has been found that when ILs are used in extractions as diluents in conjunction with appropriate extractants, the partition coefficients for lanthanides are increased compared to conventional solvents(Chun et al., 2001; Okamura et al., 2012; Rout et al., 2012). The distribution ratio of Eu(III) in CMPO-TBP/[C_4min][NTf$_2$] can be 10 times larger than when n-dodecane (n-DD)is used(Rout et al., 2011a). Nakashima et al. (2003)studied the extraction behaviour of trivalent lanthanides in the presence of CMPO/C_4mimPF$_6$, and found that use of ILs as the diluent of the extracting phase can reduce extractant consumption compared to a conventional solvent (n-DD). However, the industrial use of ionic liquidsis still limited because of their high production costs. This barrier can be overcome with the use of the small scale separators which intensify mass transfer and can lead to the reduction of the amount of solvent required.

In this work, the continuous extraction of Eu from nitric acid solutions is studied for the first time in microchannels using an ionic liquid solution (0.2M CMPO-1.2M TBP/[C_4mim][NTf$_2$]) as the extraction phase. In what follows the experimental set up and methodology are presented and the high speed imaging and bright field Particle Image Velocimetry (PIV) techniques that are used to study the hydrodynamic characteristics of the plug flow are discussed. Results are then shown on europium extraction efficiencies and mass transfer coefficients and are related to the geometric parameters of the plug flow and the circulation patterns inside the plugs. The mass transfer coefficients are also compared against literature correlations and values from conventional large scale systems.

2. Materials and experimental methodologies

In this study, the continuous extraction of Eu(III) from nitric acid solutions to a CMPO/TBP/[C_4mim][NTf$_2$] solution was carried out in 0.2 mm and 0.5 mm ID capillary channels. The ionic liquid [C_4min][NTf$_2$], with viscosity of 0.052 Pa·s and density of 1420 kg·m^{-3}, was obtained from the QUILL Research Centre, Queen's University of Belfast. The tri-n-butylphosphate (TBP), which acts as a modifier to prevent the formation of 'crud-type' precipitate (Rout et al., 2011b), was purchased from Sigma-Aldrich. CMPO was used as extractant and obtained from Carbosynth Limited. For the preparation of the ionic liquid phase, certain amount of CMPO was added into TBP and the mixture was mechanically shaken for 2 hours. Then the mixture was introduced into the ionic liquid [C_4min][NTf$_2$]and stirred. The concentrations of CMPO and TBP in the ionic liquid were equal to 0.2M and 1.2 M, respectively. Various standard nitric acid solutions were obtained from Sigma-Aldrich and used as

aqueous phase. The ionic liquid was pre-equilibrated with the desired concentration of nitric acid solution before extraction, because both H^+ and $NO3^-$ can dissolve in the IL phase. The solubility of H^+ and $NO3^-$ into the ionic liquid follows a physical absorption than a chemical extraction mechanism(Billard et al., 2011b), and neither TBP nor CMPO influence it. The fluid properties of the ionic liquid (0.2M CMPO-1.2M TBP/[C$_4$min][NTf$_2$]) and aqueous solutions (1M nitric acid) are summarized in Table 1 (measured at UCL laboratory). Each measurement was repeated 3 times to ensure reproducibility. The liquid viscosity and density were measured with a digital DV-III Ultra Rheometer (Brookfield, UK) and a DMA 5000 density meter (Anton Paar, UK), respectively. The interfacial tension was measured using a DSA 100 drop analyzer (Kruss GmbH, Germany). The refractive index was measured with an Abbe 5 Refractometer (Bellingham and Stanley, UK). The diffusion coefficient of Eu(III) in the aqueous and ionic liquid phases was obtained from the literature(Matsumiya et al., 2008; Rao et al., 2009; Ribeiro et al., 2011; Sengupta et al., 2012; Yang et al., 2014).

2.1 Experimental apparatus

A sketch of the experimental set up is shown in Fig.1. Two Kds Legato syringe pumps (KD Science Inc., USA) were used to feed the two liquid mixtures to a T-junction with an error of 1%. The aqueous phase was injected perpendicular to the channel axis and the ionic liquid phase was introduced at the axis of the main channel. A sketch of circular 0.2 mm ID microchip made of Quartz from top view is shown in Fig. 2. The main channel length (*CL*) for the 0.5 mm ID capillary varied from 5 to 25 cm. The different lengths were used to vary the residence time in the extractor without changing the mixture velocity which can affect the flow pattern. Both phases were introduced at the same volumetric flow rate which varied from $Q_{aq}=Q_{IL}$=0.653 to 21.205 ml/hr. Plug flow formed in all cases studied, with the aqueous solution forming always the dispersed plugs and the ionic liquid the continuous phase. At the channel exit, a flow splitter with a PTFE channel as the main branch and a stainless steel channel as the side branch was used to separate the two phases continuously (for details see Scheiff et al. (2011); Tsaoulidis et al. (2013)). An Asia FLLEX module (Syrris Ltd, UK) was also used as a continuous phase separator operated by adjusting the pressure differential across a hydrophobic PTFE membrane. This separator could not be used at high flow rates, though, because of high pressure drops. The separated phases were analyzed for Eu(III) concentration in a USB2000+ UV-Vis spectrometer (Ocean Optics, UK). After each set of experiments, the microchannel was cleaned with dichloromethane to remove any residual ionic liquid, then with acetone to remove any dichloromethane left. At last, compressed air was injected to the channel to ensure that all the chemicals have been cleaned. All experiments were conducted under ambient temperature (23.8-25.5°C).

High speed imaging was used to study the hydrodynamic characteristics of the two phase system (Fig. 1). A 60-Watt continuous arc lamp was used to volumetrically illuminate the microchannel from the back, and a diffuser plane was added between the backlight and the test section for uniform illumination. To minimize optical distortions, an acrylic box filled with water was put around the channel. Because of the background illumination, the interface appears as a shadow, which is captured by a high speed camera (Photron Fastcam-Ultima APX, UK) with adjustable image recording frequency from 2000 to 8000Hz depending on flowrates. The camera was coupled with an air-immersion, long working distance objective lens with magnification M=3 to 10 depending on the channel dimension. In addition, a bright field Particle Image Velocimetry technique was applied with the same optical set up to obtain the velocity profiles within the aqueous plugs. For the velocity measurements, the aqueous phase was seeded with 3μm polystyrene particles and their shadow was recorded by the high speed camera (resolution 1024X1024 pix^2). The Insight 4G (TSI instrument) software was used to pre-process and capture the images while data analysis was carried out with an in-house MATLAB code. A median filter was applied to the images to eliminate any background noise. The displacement of tracer particles between two consecutive frames was calculated to obtain velocity vectors using a square domain discretization of 32 X 32 pixels with 50% overlap to satisfy the Nyquist sampling criterion(Dore et al., 2012), with velocity spatial resolution of 26.72 μm × 26.72 μm in the 0.5 mm channel. The correlation peak position was computed with Gaussian peak algorithm detection and the validation of the velocity vectors was based on standard deviation and primary to secondary peak vectors. Removed false vectors were replaced with the median value of neighboring velocity vectors (Chinaud et al., 2015).

2.2 Chemical mechanisms

The chemical structure of [C$_4$min][NTf$_2$] ionic liquid is shown in Fig.3. The stoichiometry of metal-solvate in the ionic liquid phase varies from 1:3 (Eu : CMPO) at trace levels to 1:1 at higher Eu(III) loadings. It is determined by the slope analysis of logD_{Eu} against log[CMPO]$_{org}$(Rout et al., 2011b) , where species with overline exist in the ionic liquid phase only:

$$Eu^{3+} + \overline{xCMPO} + 3NO_3^- \leftrightarrow \overline{Eu(NO_3)_3 \cdot (CMPO)_x} \qquad (1)$$
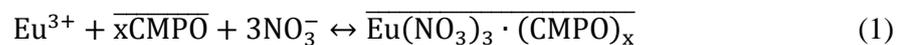
However, the equilibrium often involves ion exchange between the aqueous and the ionic liquid phases. Billard et al. (2011a) found that the cation part of the ionic liquid, C$_4$mim$^+$, was present into the aqueous phase after extraction. By dissolving C$_4$mimCl into the aqueous phase, it was shown that the presence of C$_4$mim$^+$ reduced the extraction efficiency (Nakashima et al., 2005). In some cases anion exchange was also observed, for example Tf$_2$N$^-$ transferred to aqueous Htta solution when Eu(III) was extracted from ionic liquid (Okamura et al., 2012). However, there is no clear evidence of anion exchange when ionic liquid acts as diluent, because Tf$_2$N$^-$ is a weakly coordinating anion (Binnemans, 2007). According to the

above, the mechanism can be written as:

$$Eu^{3+} + \overline{xCMPO} + 3NO_3^- + 3\overline{C_4mim^+} \leftrightarrow \overline{Eu(NO_3)_3 \cdot (CMPO)_x} + 3C_4mim^+ \qquad (2)$$
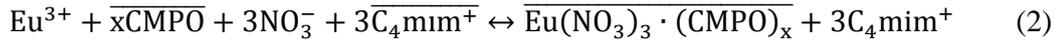
When ILs are used to recover Eu(III) in conjunction with neutral extractants, the reaction takes place in the ionic liquid phase and not in the aqueous phase as it happens with conventional solvents. Very limited research is available on the extraction kinetics of Eu(III) coupled with ionic liquid. The separations of certain rare earth metals are characterized by fast reaction but slow mass transfer using conventional organic solutions (Sarkar et al., 1980). When ionic liquids are used, however, this may not be the case due to their unique ion exchange mechanisms. Brigham (2013) investigated lanthanide extraction by HDEHP in n-dodecane from DTPA, and found that the reaction follows pseudo first- or second-order kinetics. The second order rate constant of Eu(III) extraction was about 10^4 $M^{-1}s^{-1}$, which falls into the range of fast reactions (1 to 10^{10} $M^{-1}s^{-1}$(Caldin, 2001)). Therefore the present extraction system was treated as fast reaction, although further research is still needed to accurately describe it.

3. Results and Discussion

3.1. *Specific interfacial area*

The rate of mass transfer between two phases depends on the interfacial area available. For the calculation of the interfacial area in plug flow it is assumed that the dispersed plugs have a cylindrical body and hemispherical caps at the front and back. When a continuous film is a present at the channel wall the interfacial area can be calculated as follows with an error of less than 10%(Raimondi et al., 2014):

$$\alpha_p = \frac{4W_p(L_P - w_p) + \pi W_p^2}{L_{UC}ID^2} \qquad (3)$$

where L_{uc} is the unit cell length (one slug and one plug), and W_p and L_p represent the plug width and length, respectively. The plug geometric parameters for each set of flow rates were obtained by averaging results from 30 plugs, with deviations between 4.25-7.10%for film thickness, and 5.33-9.52 % for plug and unit cell length.

The effect of mixture velocity on interfacial area can be seen in Fig.4 for equal flow rates of the two phases from $Q_{aq}=Q_{IL}$=3.534 to 21.21 ml/h. The interfacial area was found to increase slightly with increasing U_{mix}. As the mixture velocity increases the plug formation frequency increases while shorter plugs form, which results in larger interfacial area values. However, the capillary diameter has a more profound effect; the interfacial area in the large channel is almost 3 times smaller than in the small one

for the same mixture velocity. It has been suggested that the organic film can be ignored during mass transfer at low mixture velocities (Ghaini et al., 2010). However, when ionic liquid is the continuous phase the film (δ_{film}/R = 0.1585-0.3022, where δ_{film} and R are film thickness and channel radius, respectively) is thicker than with conventional organic solvents (δ_{film}/R = 0.0928-0.1295) and may affect mass transfer.

3.2. *Distribution coefficients for Eu(III) extraction*

To characterize the mass transfer process a number of parameters will be used. The Eu(III) distribution coefficient, D_{Eu}, is defined as the ratio of concentration of europium in the ionic liquid phase to the concentration in the aqueous phase:

$$D_{Eu} = \frac{c_{aq,ini} - c_{aq}^e}{c_{aq}^e} \tag{4}$$

The Eu(III) distribution coefficients for the aqueous-ionic liquid system were measured at different nitric acid concentrations (0.01, 0.1, 0.5, 1.0 and 2.0M). In the experiments, equal volumes of nitric acid solution containing europium nitrate and of ionic liquid solution (0.2M CMPO-1.2M TBP/[C$_4$min][NTf$_2$]) were mechanically shaken for 3 hours. The initial loading of Eu(III) in the aqueous phase was 20, 30 and 50 mg/mL, respectively. After equilibrium, the Eu(III) concentration was measured in the aqueous phase in a UV-Vis spectrometer. Fig.5 illustrates the Eu(III) distribution coefficient (D_{Eu}) as a function of initial nitric acid concentration ($C_{aq,ini}$). Each equilibrium experiment was repeated 5 times. The relative deviation was quite large for the low Eu(III) loading (20mg/mL), ranging between 3.69% and 28.76%, but decreased to 2.55 - 14.18% at 50 mg/mL loading, where the absorption signal in the UV-Vis is stronger and more stable than at lower loadings. The Eu(III) concentration in the ionic liquid phase was also measured with UV-Vis. The amount after extraction was between 89.65 to 101.54% of the initial Eu(III) loading. It would be difficult to have better agreement because the IL cations, the NO$_3^-$or the impurities in the imidazolium-based ionic liquids also have absorption characteristics in the UV range that can mask the Eu(III) signal (Billard et al., 2011a).

As can be seen from Fig.5 the distribution coefficient reduces with increasing Eu(III) loading, which means that the Eu(III) in the aqueous phase is more difficult to be distributed into the ionic liquid phase. However, 50 mg/mL concentration was chosen for the microchannel extraction experiments because of the low concentration measurement errors. Furthermore, the distribution coefficient has its highest value at 1.0M nitric acid concentration for all initial Eu(III) loadings, which is in agreement with the results by Rout et al. (2011b). The distribution coefficients obtained when ionic liquid is used are by a factor of 10 higher to those achieved with the conventional TUREX solvent (0.2M CMPO-1.2M TBP/n-DD) (Rout et

al., 2011a).

3.3. *Mass transfer in continuous extraction*

The performance of a mass transfer unit is characterized by the mass transfer coefficient ($K_L a$). The driving force for mass transfer will vary along the length of the microchannel and a log mean concentration difference (LMCD) can be used defined as

$$\Delta_{LMCD} = \frac{\left(C_{aq,ini}^e - C_{aq,ini}\right) - \left(C_{aq,fin}^e - C_{aq,fin}\right)}{\ln\left\{\left(C_{aq,ini}^e - C_{aq,in}\right)/\left(C_{aq,fin}^e - C_{aq,fin}\right)\right\}} \quad (5)$$

The mean value of the mass transfer flux can be written as

$$\bar{N} = K_L \Delta_{LMCD} \quad\quad\quad (6)$$

The mean value of the mass transfer flux is also equal to

$$\bar{N} = \frac{Q_{aq}\left(C_{aq,fin} - C_{aq,in}\right)}{V \alpha_p} \quad (7)$$

By combining Eqn. (6) and Eqn. (7), and integrating from the initial ($C_{aq,ini}$) to the final concentration ($C_{aq,fin}$) for time between 0 and the residence time τ, the overall mass transfer coefficient is found

$$K_L \alpha = \frac{1}{\left(1 + \frac{1}{D_{Eu}} \frac{Q_{aq}}{Q_{org}}\right)\tau} \ln\left(\frac{C_{aq,fin} - C_{aq}^e}{C_{aq,in} - C_{aq}^e}\right) \quad\quad\quad (8)$$

The extraction efficiency, E_{eff}, refers to the ratio of the amount of species transferred to the maximum amount transferable:

$$E_{eff} = \frac{\text{Amount transferred}}{\text{Maximum amount transferable}} = \frac{C_{aq,in} - C_{aq,fin}}{C_{aq,in} - C_{aq}^e} \quad\quad\quad (9)$$

The efficiency is a good indicator of the mass transfer performance of the contactor at various contact times (Bapat and Tavlarides, 1985; Dehkordi, 2001). The extraction efficiency depends not only on the overall volumetric mass transfer coefficient ($K_L a$) but also on the residence time (τ).

The overall volumetric mass transfer coefficients of the Eu(III) extraction in the 0.5 mm ID microchannel, calculated from Eqn. (8), are shown in Fig.6a as a function of residence time. To obtain different residence times (τ), the channel length was varied from 5 cm, 15 cm to 25 cm, at the same volumetric flow rates of the two liquids $Q_{aq} = Q_{IL} = 3.534$ ml/hr. The volumetric mass transfer coefficient was found to decrease non-linearly with increasing residence time. On average, the mass transfer coefficient of $\tau=10$s (*CL*=5 cm) was 1.5 times higher than that of $\tau=30$ s (*CL*=15 cm) under all nitric acid solutions, while the change between $\tau=30$ s and $\tau=50$ s (*CL*=25 cm) was small. This suggests that the mass transfer at the inlet of the channel contributes significantly to the overall mass transfer in the separation unit. The nitric acid

concentration affects the mass transfer coefficient in a similar way that it affects the distribution coefficient (Fig. 5). The highest mass transfer was found at 1.0M nitric acid concentration, followed by the 0.5 and 2.0 M concentrations. The lowest K_La were found for 0.1M nitric acid concentration.

The effect of residence time on extraction efficiency can be seen in Fig.6b. In all cases the extraction efficiency increases with residence time. In the shortest channel (CL=5 cm and τ=10 s) the extraction efficiency is relatively low (43.55%) despite the high mass transfer coefficients. The highest E_{eff} was found at 1M nitric acid concentration and at the longest residence time, where it reaches 71.50% of the equilibrium value.

3.4. *Effect of mixture velocity on Eu(III) microfluidic extraction*

The effect of mixture velocity on overall volumetric mass transfer coefficient was investigated in the 0.5mm ID microchannel (CL=15 cm) at varying nitric acid concentrations, for equal volumetric flow rates of the two phases ranging from $Q_{aq}=Q_{IL}$=3.534 to 21.21 ml/hr. As can be seen in Fig.7 for 1M nitric acid concentration the mass transfer coefficient increases with increasing mixture velocity, which means the extraction system is mass transfer dominated. The increase in the mass transfer coefficient is partly attributed to the small increase in interfacial area (see Fig.4). This contribution, however, is small; for example the area increases by 4.64% when the mass transfer coefficient rises by 54% for change in velocity from 0.5 to 3 cm/s. Mixture velocity, affects mass transfer in plug flow via two mechanisms:(a) convection due to internal circulation in the plugs and slugs; (b) molecular diffusion due to concentration gradients adjacent to the interface (Kashid et al., 2007; Dessimoz et al., 2008). The increase in mixture velocity increases the intensity of internal circulation and enhances convective mass transfer (Tsaoulidis and Angeli, 2015). The circulation also helps interface renewal that increases the concentration gradients and therefore mass transfer close to the interface. The mass transfer performance, however, does not depend only on mixture velocity and as can be seen at nitric acid concentration different from 1M, the effect of mixture velocity on the mass transfer coefficient is less significant. The extraction of Eu(III) is a physical process combined with chemical reaction, and depends on both mass transfer and intrinsic reaction kinetics (Xu et al., 2013).

To evaluate the role of film thickness on mass transfer, van Baten and Krishna (2004) proposed different correlations for mass transfer from the plug caps and the film in the plug flow regime:

$$K_{L,cap} = 2\frac{\sqrt{2}}{\pi}\sqrt{\frac{DU_P}{d_c}} \tag{10}$$

$$K_{L,film} = 2\sqrt{\frac{D}{\pi t_{film}}}\frac{ln(1/\Delta)}{(1-\Delta)}; \quad Fo< 0.1 \text{ (short contact)} \tag{11}$$

$$K_{L,film} = 3.41 \frac{D}{\delta_{film}}; \quad Fo > 0.1 \text{ (long contact)} \tag{12}$$

$$K_L \alpha = K_{L,cap} \alpha_{cap} + K_{L,film} \alpha_{film} \tag{13}$$

where the Fourier number (Fo) is defined as $Fo = D/t_{film} \delta_{film}^2$, and Δ is a dimensionless parameter based on Fo. The plug velocity, U_p, is obtained based on the plug displacement from the high speed imaging. The contact time of the liquid film, $t_{film} = L_{film} /(U_p + U_{film})$, is calculated under the assumption that the film velocity is nearly negligible in the microchannel. The mass transfer via the film can be evaluated depending on the value of the Fourier number (Fo), where $Fo < 0.1$ and $Fo > 0.1$ for short and long contact time respectively. The aqueous plug in the present work shows long film contact times as Fo ranges between 0.486 and 1.235. The Eu(III) $K_{L,film}$ in the 0.2 mm ID channel was found to decrease from 4.702 to 3.353×10^{-7} m·s^{-1} when U_{mix} increased from 0.01 to 0.06 m/s, and $K_{L,cap}$ increased from 1.151 to 2.985×10^{-5} m·s^{-1} under the same operation conditions. These results show that 99% Eu(III) is extracted via the cap regions, and the film region has a minor effect on the overall mass transfer. It explains why high $K_L a$ occurs at larger U_{mix}, where plug formation frequency increases and shorter plugs form, which would result in increased cap regions that enhance mass transfer. At $U_{mix} > 0.04$ m/s where $Fo > 0.8$ and $\Delta \approx 0$ (van Baten and Krishna (2004)), the ionic liquid film approaches saturation, and its contribution to the overall mass transfer becomes insignificant.

The Eu(III) extraction efficiency is shown in Fig. 8 for the 0.5 mm ID microchannel ($CL = 15$ cm). The extraction efficiency increases with increasing residence time (decreasing mixture velocity). The highest extraction efficiencies are obtained for 1M nitric acid concentration similar to distribution coefficients (see Fig. 5). Although the mass transfer coefficient at $U_{mix} = 3$ cm/s has the highest values, the corresponding extraction efficiencies are only 36.24% to 58.13% of the equilibrium value due to the short residence times ($\tau = 5$s).

3.5. *Effect of capillary size on Eu(III) extraction*

The effect of channel size on overall volumetric mass transfer coefficient is shown in Fig.9 for 0.2 and 0.5 mm ID capillaries as a function of mixture velocity at the same channel length ($CL = 25$ cm). 1M nitric acid was used as aqueous phase, and equal flow rates of the both phases were used varying from 0.065 to 14.14ml/h. Generally, $K_L a$ are higher in the small channel because of the large interfacial area compared to the 0.5 mm channel. As depicted in Fig.4, the average interfacial area increases from 3600 m^2/m^3 to 8250 m^2/m^3 when the capillary internal diameter reduces from 0.5mm to 0.2mm. The difference between the mass transfer coefficients increases with mixture velocity. For example, at $U_{mix} = 1$ cm/s the difference is about 10.5% of the 0.5 mm channel $K_L a$, but increases to 21.4% at $U_{mix} = 3$ cm/s. The increased surface

10

renewal rate and recirculation intensity caused by higher plug velocities in the small channel are considered to be responsible for the difference. In fact, the plug velocity is always higher than the mixture velocity in the liquid-liquid plug flow regime, due to the existence of a nearly stagnant ionic film surrounding the aqueous phase plug. The non-dimensional film thickness (δ_{film}/R) in the 0.2 mm ID channel was found to be 8.47-32.92% larger than in the 0.5 mm ID channel from the imaging experiments, depending on the mixture velocity. Therefore the enclosed plug moves slightly faster in the small channel. This is also confirmed by the imaging experiments, which showed that plugs in the 0.2 mm ID channel moved5.94- 17.74% faster compared to the large channel.

3.6. *Effect of recirculation intensity on Eu(III) microfluidic extraction*

The convective mass transfer inside the plugs is strongly affected by the recirculation patterns, which are caused by the shear between the continuous phase and the plug axis. To obtain the recirculation patterns, for each set of conditions the instantaneous velocity profiles of 30 plugs were averaged, with a deviation of 4.35-9.99%. The average plug velocity was then calculated by integrating the laminar velocity profiles of the averaged velocity field along the plug length. The recirculation pattern was finally obtained by subtracting the average velocity from the local velocities in the plug. An example of the averaged recirculation pattern inside a plug is shown in Fig. 10afor $Q_{aq}=Q_{IL}$=3.534 ml/hr. It consists of two counter rotating vortices with closed streamlines and symmetrical about the channel axis. The recirculation intensity within the plug is characterized by the recirculation time which is the time needed to displace material from one to the other end of the plug (Thulasidas et al., 1997; Kececi et al., 2009; Dore et al., 2012). A two-dimensional recirculation time was calculated as follows (Dore et al., 2012):

$$\tau(x) = \frac{L_P y_0}{\int_0^{y_0} u(x,y) dy} \cong \frac{L_P y_0}{\Delta \sum_{i=1}^{i=N} u_i|x} \tag{14}$$

where y_o is the location of the stagnation point projected onto the observation mid-plane. As can be seen from Fig. 10b the recirculation time is almost constant in the middle of the channel but increase towards the front and back ends of the plug where the streamlines are not well defined. The recirculation time is usually treated as constant inside the liquid plug(Thulasidas et al., 1997; Kashid et al., 2005; Tsoligkas et al., 2007). However, Dore et al. (2012)experimentally found that the circulation pattern may not be fully symmetric, especially at shorter plugs.

The recirculation times averaged for the middle part of the plug are plotted in Fig. 11 against the plug travel time, in the 0.5mm ID channel for $Q_{aq}=Q_{IL}$=3.534 to 21.21 ml/hr. The plug travel time is defined as the time needed by the liquid plug to travel a distance of its own length, given by $T_p=L_p/U_{mix}$, where L_p is the plug length. The corresponding mass transfer coefficients are also plotted. As discussed above, high

mixture velocities (U_{mix}) result in shorter plug lengths, thus leading to a shorter plug travel time (T_p). In shorter plugs, decreased recirculation times are observed, which means the fluid in the plug will experience a larger number of revolutions and better mixing. This is supported by the increase in the mass transfer coefficient at low T_p, where the circulation time is also short. A similar trend was also observed by Kashid et al. (2005)who argued that high mixture velocities increase recirculation intensity because of increased shear between the wall surface and the plug. Meanwhile, higher mixture velocity increases the thickness of the film surrounding the plug and decreases the plug diameter, which results in a shorter path length for the Eu(III) diffusion in the radial direction that also helps mass transfer.

3.7. Comparison of K_La with correlations

Mass transfer in multiphase small scale units is a complex process, which depends not only on the hydrodynamic characteristics but also on the kinetics of the species transfer. Several models have been proposed to estimate mass transfer coefficients in gas-liquid and liquid-liquid plug flow either empirical or developed from the film and penetration theories. Bercic and Pintar (1997) suggested a correlation, Eqn.(15), for gas-liquid flow which considers only the contribution of the plug caps since, as the authors argued, the film becomes quickly saturated. This model was able to predict accurately $k_L\alpha$ for long bubbles and liquid slugs. Vandu et al. (2005) suggested a model for the mass transfer coefficient where the dominant contribution was from the film (Eqn. 16). A constant was introduced whose value was estimated from the best fitting of experimental data from different unit cell lengths L_{UC}, gas hold up ε_G and rise velocity U_p. Yue et al. (2009) proposed an empirical correlation (Eqn. 17) suitable for short films and non-uniform concentration in the plugs, which differs from the well mixed assumption of the previous models. Similarly, Kashid et al. (2010) developed an empirical correlation (Eqn. 18) specifically for liquid-liquid plug flow as a function of Reynolds number, Capillary number, diameter and length of the capillary. The correlation was able to predict the experimental data within 95% even when the density, viscosity and interfacial tension of the aqueous phase was changed with the addition of surfactants.

The mass transfer coefficients measured in 0.2 and 0.5mm ID channels are compared with these correlations in Fig.12.The fitting parameters in the correlations byVandu et al. (2005) (Eqn.16), Yue et al. (2009)(Eqn. 17) and Kashid et al. (2010) (Eqn. 18) were determined from least square regression analysis of the data in both channels:

$$k_L\alpha = 0.111 \frac{(U_p+U_s)^{1.19}}{((1-\varepsilon_G)L_{UC})^{0.57}} \quad \text{(15; Bercic and Pintar, 1997)}$$

$$k_L\alpha = 3.65 \sqrt{\frac{DU_p}{L_{UC}}} \frac{1}{ID} \quad \text{(16; Vandu et al., 2005)}$$

$$k_L a = \frac{1.67}{ID} \left(\frac{U_p}{ID}\right)^{0.5} \left(\frac{L_p}{ID}\right)^{0.15} \left(\frac{L_p+L_S}{ID}\right)^{0.05} \quad \text{(17; Yue et al, 2009)}$$

12

$$k_L \alpha \frac{L_p}{u_{mix}} = 0.0257 Ca^{-0.6} Re^{0.05} \left(\frac{ID}{L_p}\right)^{-0.1} \quad \text{(18; Kashid et al, 2010)}$$

The model suggested by Bercic and Pintar (1997) shows deviations as high as 55.41% compared to the experiment results. This correlation does not include the effect of channel size, and it was developed for velocities higher than those used in this work. Besides, the liquid slug length (3-13.5 cm) and unit cell length (1.7-22 cm) considered for the model development were about 100 times larger than in the current work. The model byVandu et al. (2005)gives better predictions particularly for the large channel with standard deviation varying from 11.53 to 42.12%. The correlation was in fact developed for gas-liquid flow in 1-3 mm ID capillaries, for bubbles and liquid slugs longer ($L_{UC}=5-60$ mm) than in the present work ($L_{UC}=0.314$-1.153 mm). The predictions of the two empirical correlations (Eqn. 17 and 18) are better, with deviations less than 20%. The model by Yue et al. (2009) (standard deviation 5.35-16.72%) was developed based on the physical absorption of oxygen from rising air bubbles into water in square microchannels with ID=0.4 mm. The differences from the current data may be attributed to the low mass transfer resistance in the gas phase bubbles compared to liquid plugs. The model by Kashid et al. (2010) which was developed from liquid-liquid systems agrees best with the experiment results (standard deviations 5.16 -11.88%). Empirical correlations may agree better with the experimental data because the effects of chemical reaction kinetics and inlet junction configuration can be included in the constants, while such effects are not taken into account in the models based on film and penetration theory on a fully formed plug (Eqn.15 and Eqn.16).

Preliminary Eu(III) extraction experiments were carried out with cyclohexane as organic phase diluent for comparison in the 0.5 mm ID channel. The Eu(III) was extracted with 50% TBP in cyclohexane from 2 M nitric acid, and the distribution coefficient was found to be between 0.024 and 0.041. Under the same flow rate of both phases, the $K_L a$ of the cyclohexane system (0.0262-0.0643s^{-1}) was similar to that of the ionic liquid system (0.0339-0.0602s^{-1}). However, the Eu(III) initial loading when cyclohexane was used was only 0.31 mg/mL (2×10^{-3} M), because of the low limiting organic concentration (LOC). In conventional systems like n-DD or cyclohexane as organic diluent, the LOC of europium is 9 mg/mL; beyond this concentration the organic phase will split into two phases a heavier (rich in metal-solvate) and a lighter phase (rich in diluent) called third phase formation. This is not observed when the ionic liquid is used, even when the loading of Eu(III) in the ionic liquid phase increased from 12 to 40 mg/mL (Rout et al., 2011a). Therefore the high process capacity is an additional benefit of the present system.

The mass transfer coefficients and interfacial areas found in this work are compared against those from other microfluidic units and conventional extract ion units in Table 2. For the comparisons of $K_L a$ values in microfluidic system, previous studies using different liquid-liquid extraction systems are listed as well.

As can be seen, the interfacial areas are comparable to those obtained in other microfluidic systems but significantly higher than those in conventional extraction units. The mass transfer coefficients are again higher than the ones achieved in conventional extractors but not as high as those in different microfluidic applications. This may be due to the low distribution coefficients found for the Eu(III) extraction.

4.   Conclusions

The intensified extraction of Eu from nitric acid solutions into an ionic liquid phase 0.2M CMPO-1.2M TBP/[C_4mim][NTf_2] was studied experimentally in small channels with diameters 0.2 and 0.5 mm. Experiments were carried out in the plug flow regime, where the aqueous solution formed the dispersed plugs and the ionic liquid solution was the continuous phase. Phase equilibrium studies showed that the distribution coefficients had the highest value at nitric acid concentration equal to 1M. The geometric characteristics of the flow pattern (plug length, film thickness and interfacial area) were investigated with high speed imaging while velocity fields within the aqueous phase plugs were obtained using high speed bright field micro PIV.

The results revealed that the interfacial areas and the mass transfer coefficients were significantly higher than in conventional contactors. In addition, $K_L a$ were found to be higher in the small channel compared to the large one for the same mixture velocities, as a result of large interfacial areas and reduced circulation times. Within the same channel, the mass transfer coefficients increased and then decreased with increasing nitric acid concentration in accordance with the partition coefficients. The mass transfer coefficients were also found to decrease with residence time suggesting that significant mass transfer occurs at the channel inlet. The mixture velocity affected the mass transfer coefficient particularly in the case of 1M nitric acid concentration. The circulation times within the plugs, calculated from the detailed velocity profiles, were found to decrease with decreasing plug size and increasing mixture velocity; small circulation times result in better mixing and mass transfer. The empirical correlation suggested by Kashid et al. (2010) was able to predict the current results (with deviations 5.16-11.88%) better than other literature correlations.

Nomenclature

Latin Symbols

Ca	Capillary number, Ca=$\frac{\mu_{IL} U_{mix}}{\gamma}$, dimensionless
$C_{aq,ini}$	initial concentration of Eu(III) in aqueous phase, mol·L^{-1}

$C_{aq,fin}$	final concentration of Eu(III) in aqueous phase, mol·L⁻¹
C_{aq}^e	Eu(III) concentration in aqueous phase at equilibrium, mol·L⁻¹
C(HNO₃)	nitric acid concentration, M
CL	channel length, cm
D	Eu(III) diffusion coefficient, m²· s⁻¹
D_{Eu}	Eu(III) distribution coefficient
E_{eff}	extraction efficiency, %
K_L	overall mass transfer coefficient, m·s⁻¹
K_La	overall volumetric mass transfer coefficient, s⁻¹
$K_{L,cap}$	mass transfer via cap, s⁻¹
$K_{L,film}$	mass transfer via film, s⁻¹
L_{film}	film length, m
L_P	plug length, m
L_s	slug length, m
L_{UC}	length of unit cell, m
n	Refractive index, dimenionless
N	mass transfer flux, mol m⁻²·s⁻¹
Q_{aq}	volumetric flow rate of aqueous phase, ml·h⁻¹
Q_{IL}	volumetric flow rate of ionic liquid phase, ml·h⁻¹
ID	channel internal diameter, mm
R	channel internal radius, mm
Re	Reynolds number, $Re=\frac{\rho U_{mix}ID}{\mu}$, dimensionless
t_{film}	Contact ime of liquid film, s
U_{mix}	mixture velocity, cm·s⁻¹
U_p	plug velocity, cm·s⁻¹
U_{film}	film velocity, cm·s⁻¹
W_p	plug width, m

Greek Symbols

α_p	plug interfacial area, m²·m⁻³
ρ	density, kg·m⁻³
τ	residence time, s
δ_{film}	film thickness, mm
μ	dynamic viscosity, cp
γ	Interfacial tension, mN·m⁻¹
Δ	dimensionless parameter
Δ_{LMCD}	log mean concentration difference, mol·m⁻³

Acknowledgements

References

Alper, E., 1988. Effective interfacial area in the RTL extractor from rates of extraction with chemical reaction. Chemical engineering research & design 66, 147-151.

Assmann, N., Ładosz, A., Rudolf von Rohr, P., 2013. Continuous Micro Liquid-Liquid Extraction. Chemical Engineering & Technology 36, 921-936.

Bapat, P., Tavlarides, L., 1985. Mass transfer in a liquid-liquid CFSTR. AIChE Journal 31, 659-666.

Bercic, G., Pintar, A., 1997. The role of gas bubbles and liquid slug lengths on mass transport in the Taylor flow through capillaries. Chemical Engineering Science 52, 3709-3719.

Billard, I., Ouadi, A., Gaillard, C., 2011a. Liquid–liquid extraction of actinides, lanthanides, and fission products by use of ionic liquids: from discovery to understanding. Anal Bioanal Chem 400, 1555-1566.

Billard, I., Ouadi, A., Jobin, E., Champion, J., Gaillard, C., Georg, S., 2011b. Understanding the Extraction Mechanism in Ionic Liquids: UO22+/HNO3/TBP/C4-mimTf2N as a Case Study. Solvent Extraction and Ion Exchange 29, 577-601.

Binnemans, K., 2007. Lanthanides and actinides in ionic liquids. Chemical reviews 107, 2592-2614.

Brigham, D.M., 2013. Lanthanide-Polyaminopolycarboxylate Complexation Kinetics in High Lactate Media: Investigating the Aqueous Phase of TALSPEAK. WASHINGTON STATE UNIVERSITY.

Burns, J.R., Ramshaw, C., 2001. The intensification of rapid reactions in multiphase systems using slug flow in capillaries. Lab Chip 1, 10-15.

Caldin, E., 2001. The mechanisms of fast reactions in solution. IOS Press.

Chinaud, M., Roumpea, E.-P., Angeli, P., 2015. Studies of plug formation in microchannel liquid–liquid flows using advanced particle image velocimetry techniques. Experimental Thermal and Fluid Science 69, 99-110.

Chun, S., Dzyuba, S.V., Bartsch, R.A., 2001. Influence of Structural Variation in Room-Temperature Ionic Liquids on the Selectivity and Efficiency of Competitive Alkali Metal Salt Extraction by a Crown Ether. Anal Chem 73, 3737-3741.

De Morais, C., 2000. Recovery of europium and yttrium from color TV tubes, 55 Congresso Anual Associacao Brasileria de Metalurgia e Materiais, Rio de Janeiro, Brazil.

Dehkordi, A.M., 2001. Novel Type of Impinging Streams Contactor for Liquid−Liquid Extraction. Industrial & Engineering Chemistry Research 40, 681-688.

Dehkordi, A.M., 2002. Liquid-liquid extraction with an interphase chemical reaction in an air-driven two-impinging-streams reactors: Effective interfacial area and overall mass-transfer coeffcient. Ind. Eng.Chem. Res 41, 4085-4093.

Dessimoz, A.-L., Cavin, L., Renken, A., Kiwi-Minsker, L., 2008. Liquid–liquid two-phase flow patterns and mass transfer characteristics in rectangular glass microreactors. Chemical Engineering Science 63, 4035-4044.

Dore, V., Tsaoulidis, D., Angeli, P., 2012. Mixing patterns in water plugs during water/ionic liquid segmented flow in microchannels. Chemical Engineering Science 80, 334-341.

Fernandes, J.B., Sharma, M.M., 1967. Effective interfacial area in agitated liquid—liquid contactors. Chemical Engineering Science 22, 1267-1282.

Ghaini, A., Kashid, M.N., Agar, D.W., 2010. Effective interfacial area for mass transfer in the liquid–liquid slug flow capillary microreactors. Chemical Engineering and Processing: Process Intensification 49, 358-366.

Goonan, T.G., 2011. Rare Earth Elements--end Use and Recyclability. US Department of the Interior, US Geological Survey.

Horwitz, E.P., Kalina, D.G., Kaplan, L., Mason, G.W., Diamond, H., 1982. Selected Alkyl(phenyl)-N,N-dialkylcarbamoylmethylphosphine Oxides as Extractants for Am(III) from Nitric Acid Media. Separation Science and Technology 17, 1261-1279.

Jovanović, J., Rebrov, E.V., Nijhuis, T.A., Kreutzer, M.T., Hessel, V., Schouten, J.C., 2012. Liquid–Liquid Flow in a Capillary Microreactor: Hydrodynamic Flow Patterns and Extraction Performance. Industrial & Engineering Chemistry Research 51, 1015-1026.

Kashid, M.N., Gupta, A., Renken, A., Kiwi-Minsker, L., 2010. Numbering-up and mass transfer studies of liquid–liquid two-phase microstructured reactors. Chemical Engineering Journal 158, 233-240.

Kashid, M.N., I.Gerlach, S.Goetz, J.Franzke, J.F.Acker, F.Platte, D.W.Agar, S.Turek, 2005. Internal

circulation within the liquid slugs of a liquid–liquid slug-flow capillary microreactor. Industrial&Engineering Chemistry Research 2005, 5003-5010.

Kashid, M.N., Platte, F., Agar, D., Turek, S., 2007. Computational modelling of slug flow in a capillary microreactor. Journal of Computational and Applied Mathematics 203, 487-497.

Kececi, S., Wörner, M., Onea, A., Soyhan, H.S., 2009. Recirculation time and liquid slug mass transfer in co-current upward and downward Taylor flow. Catalysis Today 147, S125-S131.

Khakpay, A., Abolghasemi, H., Salimi-Khorshidi, A., 2009. The effects of a surfactant on mean drop size in a mixer-settler extractor. Chemical Engineering and Processing: Process Intensification 48, 1105-1111.

Kiwi-Minsker, L., Renken, A., 2005. Microstructured reactors for catalytic reactions. Catalysis Today 110, 2-14.

Kučera, J., Mizera, J., Řanda, Z., Vávrová, M., 2007. Pollution of agricultural crops with lanthanides, thorium and uranium studied by instrumental and radiochemical neutron activation analysis. Journal of Radioanalytical and Nuclear Chemistry 271, 581-587.

Lee, C.-J., Yang, B.-R., 1995. Extraction of trivalent europium via a supported liquid membrane containing PC-88A as a mobile carrier. The Chemical Engineering Journal and the Biochemical Engineering Journal 57, 253-260.

Lew, K., 2010. The 15 Lanthanides and the 15 Actinides. The Rosen Publishing Group, 30.

Löwe, H., Ehrfeld, W., 1999. State-of-the-art in microreaction technology: concepts, manufacturing and applications. Electrochimica Acta 44, 3679-3689.

Matsumiya, M., Suda, S., Tsunashima, K., Sugiya, M., Kishioka, S.-y., Matsuura, H., 2008. Electrochemical behaviors of multivalent complexes in room temperature ionic liquids based on quaternary phosphonium cations. Journal of Electroanalytical Chemistry 622, 129-135.

Nakashima, K., Kubota, F., Maruyama, T., Goto, M., 2003. Ionic liquids as a novel solvent for lanthanide extraction. Analytical Sciences 19, 1097-1098.

Nakashima, K., Kubota, F., Maruyama, T., Goto, M., 2005. Feasibility of ionic liquids as alternative separation media for industrial solvent extraction processes. Industrial & Engineering Chemistry Research 44, 4368-4372.

Okamura, H., Sakae, H., Kidani, K., Hirayama, N., Aoyagi, N., Saito, T., Shimojo, K., Naganawa, H., Imura, H., 2012. Laser-induced fluorescence and infrared spectroscopic studies on the specific solvation of

tris(1-(2-thienyl)-4,4,4-trifluoro-1,3-butanedionato)europium(III) in an ionic liquid. Polyhedron 31, 748-753.

Okubo, Y., Maki, T., Aoki, N., Hong Khoo, T., Ohmukai, Y., Mae, K., 2008. Liquid–liquid extraction for efficient synthesis and separation by utilizing micro spaces. Chemical Engineering Science 63, 4070-4077.

Puranik, S., Sharma, M., 1970. Effective interfacial area in packed liquid extraction columns. Chemical Engineering Science 25, 257-266.

Rabah, M.A., 2008. Recyclables recovery of europium and yttrium metals and some salts from spent fluorescent lamps. Waste management 28, 318-325.

Raimondi, N.D.M., Prat, L., Gourdon, C., Tasselli, J., 2014. Experiments of mass transfer with liquid–liquid slug flow in square microchannels. Chemical Engineering Science 105, 169-178.

Rao, C.J., Venkatesan, K., Nagarajan, K., Srinivasan, T., Rao, P.V., 2009. Electrochemical behavior of europium (III) in N-butyl-N-methylpyrrolidinium bis (trifluoromethylsulfonyl) imide. Electrochimica Acta 54, 4718-4725.

Resende, L.V., Morais, C.A., 2010. Study of the recovery of rare earth elements from computer monitor scraps – Leaching experiments. Minerals Engineering 23, 277-280.

Ribeiro, A., Valente, A., Lobo, V., 2011. Diffusion behaviour of trivalent metal ions in aqueous solutions. Chemistry and Chemical Technology 5.

Rout, A., Venkatesan, K.A., Srinivasan, T.G., Vasudeva Rao, P.R., 2011a. Extraction and third phase formation behavior of Eu(III) IN CMPO–TBP extractants present in room temperature ionic liquid. Separation and Purification Technology 76, 238-243.

Rout, A., Venkatesan, K.A., Srinivasan, T.G., Vasudeva Rao, P.R., 2011b. Room temperature ionic liquid diluent for the extraction of Eu(III) using TRUEX extractants. Journal of Radioanalytical and Nuclear Chemistry 290, 215-219.

Rout, A., Venkatesan, K.A., Srinivasan, T.G., Vasudeva Rao, P.R., 2012. Extraction behavior of actinides and fission products in amide functionalized ionic liquid. Separation and Purification Technology 97, 164-171.

Sarkar, S., Mumford, C.J., Phillips, C.R., 1980. Liquid-Liquid Extraction with Interphase Chemical Reaction in Agitated Columns. 1. Mathematical Models. Industrial & Engineering Chemistry Process Design and Development 19, 665-671.

Scheiff, F., Mendorf, M., Agar, D., Reis, N., Mackley, M., 2011. The separation of immiscible liquid slugs within plastic microchannels using a metallic hydrophilic sidestream. Lab Chip 11, 1022-1029.

Schulz, W., Horwitz, E., 1986. Recent progress in the extraction chemistry of actinide ions. Journal of the Less Common Metals 122, 125-138.

Sen, N., Darekar, M., Singh, K., Mukhopadhyay, S., Shenoy, K., Ghosh, S., 2014. Solvent extraction and stripping studies in microchannels with TBP nitric acid system. Solvent Extraction and Ion Exchange 32, 281-300.

Sengupta, A., Mohapatra, P.K., Iqbal, M., Verboom, W., Huskens, J., Godbole, S.V., 2012. Extraction of Am(iii) using novel solvent systems containing a tripodal diglycolamide ligand in room temperature ionic liquids: a 'green' approach for radioactive waste processing. RSC Advances 2, 7492.

Sukhamoy Sarkar, J.Mumford, C., R.Phillips, C., 1980. Liquid-liquid extraction with an interphase chemical reaction in agitated columns.1. Mathmatical models. Industrial& Engineering Chemistry Process Design and Development 19, 665-671.

Thulasidas, T., Abraham, M., Cerro, R., 1997. Flow patterns in liquid slugs during bubble-train flow inside capillaries. Chemical Engineering Science 52, 2947-2962.

Tsaoulidis, D., Angeli, P., 2015. Effect of channel size on liquid-liquid plug flow in small channels. AIChE Journal, n/a-n/a.

Tsaoulidis, D., Dore, V., Angeli, P., Plechkova, N.V., Seddon, K.R., 2013. Dioxouranium(VI) extraction in microchannels using ionic liquids. Chemical Engineering Journal 227, 151-157.

Tsoligkas, A.N., Simmons, M.J.H., Wood, J., 2007. Influence of orientation upon the hydrodynamics of gas–liquid flow for square channels in monolith supports. Chemical Engineering Science 62, 4365-4378.

Vandu, C.O., Liu, H., Krishna, R., 2005. Mass transfer from Taylor bubbles rising in single capillaries. Chemical Engineering Science 60, 6430-6437.

Verma, R., Sharma, M., 1975. Mass transfer in packed liquid—liquid extraction columns. Chemical Engineering Science 30, 279-292.

Wang, G., Peng, Q., Li, Y., 2011. Lanthanide-doped nanocrystals: synthesis, optical-magnetic properties, and applications. Accounts of chemical research 44, 322-332.

Kashid, M.N., Harshe, Y.M., Agar D.W.,2007. Liquid-liquid slug flow in capillary: an alternative to suspended drop or film contactors. Industrial &Engineering Chemistry Research 46, 8420-8430.

Kashid, M.N., Renken, A. Kiwi-Minsker, L., 2011. Influence of flow regime on mass transfer in different types of microchannels. Industrial &Engineering Chemistry Research 50, 6906-6914.

Xu, B., Cai, W., Liu, X., Zhang, X., 2013. Mass transfer behavior of liquid–liquid slug flow in circular cross-section microchannel. Chemical Engineering Research and Design 91, 1203-1211.

Yang, L., Zhao, Y., Su, Y., Chen, G., 2013. An Experimental Study of Copper Extraction Characteristics in a T-Junction Microchannel. Chemical Engineering & Technology 36, 985-992.

Yang, X., He, L., Qin, S., Tao, G.-H., Huang, M., Lv, Y., 2014. Electrochemical and Thermodynamic Properties of Ln(III) (Ln = Eu, Sm, Dy, Nd) in 1-Butyl-3-Methylimidazolium Bromide Ionic Liquid. PLoS ONE 9, e95832.

Yue, J., Luo, L., Gonthier, Y., Chen, G., Yuan, Q., 2009. An experimental study of air–water Taylor flow and mass transfer inside square microchannels. Chemical Engineering Science 64, 3697-3708.

Tables

Table 1

Properties of the test fluids

Property/parameter (25ºC)	Fluid/value
Density (ρ)/[kg/m^3]	Ionic liquid phase: 1259
	Aqueous phase: 1030
Dynamic viscosity (μ)/[cp]	Ionic liquid phase: 25.59
	Aqueous phase: 0.75
Interfacial tension(γ)/[mN/m]	Ionic liquid phase /Aqueous phase =6.70
Eu(III) diffusion coefficient(D)/[m$^2\cdot$ s^{-1}]	Ionic liquid phase: 2.95×10^{-12}
	Aqueous phase: 7.86×10^{-8}
Refractive index(n)	Ionic liquid phase: 1.427
	Aqueous phase: 1.339
	FEP channel: 1.34
	Deionized water: 1.335

Table 2

Comparison of K_La values in liquid-liquid microfluidic systems using T/Y-junctions

Liquid-liquid contactor	System	K_La (s^{-1})	α (m^2 m^{-3})	Reference
T-junction capillaries, ID=0.2 and 0.5mm	0.2M CMPO-1.2M TBP/[C$_4$mim][NTf$_2$]---1M nitric acid	0.005-0.05	3750-8250	Present work
T-junction capillaries, ID= 0.5mm	50% TBP in cyclohexane---1M nitric acid	0.0262-0.0643	3613-3979	Present work
Soda-lime glass 0.38mm depth chip	Kerosene/acetic acid/ water+NaOH	Order of magnitude of 0.5	N/A	Burns and Ramshaw (2001)
PTFE capillary with Y-junction, 0.5, 0.75 and 1mm	Kerosene/n-butanol/water	0.02-0.31	590-4800	Kashid et al.(2007)
Rectangular glass microchannel 0.4mm	Hexane trichloroacetic acid/ water+NaOH	0.2-0.5	10700-11200	Dessimoz et al. (2008)
Capillary microreactor, ID=0.5mm	n-butyl formate-aqueous NaOH solution	0.90-1.67	1600-3200	Ghaini et al. (2010)
Square (glass, 0.4mm), T-square (glass, 0.4mm), T-trapezoidal, 0.269mm), Y-rectangular (0.15mm ID), Concentric (glass, 0.15mm)	Nonreacting water-acetone – toluene	0.01-0.74	N/A	Kashid et al. (2011)
Opposed T-junction, ID=0.6, 0.8 and 1.0mm	Sodium hydroxide---n-butyl acetate	0.006-0.37	1300-4100	Xu et al. (2013)
T-junction Teflon channel, ID=0.5mm	30%TBP in [C$_4$mim][NTf$_2$]---3M nitric acid	0.049-0.312	N/A	Tsaoulidis et al. (2013)
T-junction, PTFE capillary with 2mm ID, 0.0016 to 0.45m/s	CuSO$_4$/H$_2$SO$_4$/AD-100/260#	0.03-0.26	N/A	Yang et al. (2013)

T-junction serpentine microchannel , ID=0.278 and 0.319 mm	30% TBP in dodecane (nitric acid)--- water	0.001-4	N/A	Sen et al. (2014)
Square Glass T-junction microchannel , 210 μm	Water/acetone/toluene	1.61-8.44	6090-13400	Raimondi et al. (2014)
Packed extraction columns	n-butyl formate-aqueous NaOH solution	0.0034-0.005	80-450	Verma and Sharma (1975)
RTL extractors (Graesser raining bucket)	n-butyl formate-aqueous NaOH solution	$(0.6\text{-}1.3)\times10^{-6}$	90-140	Alper (1988)
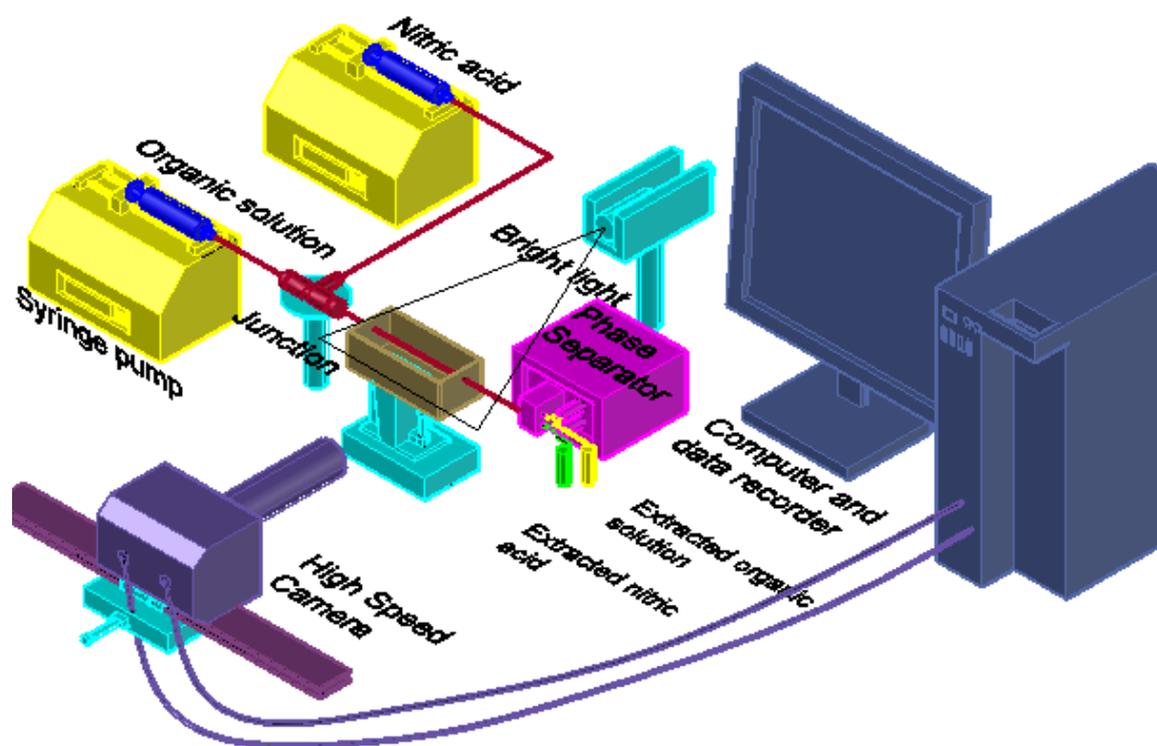
Fig.1. Sketch of the experimental set up including the high speed imaging system
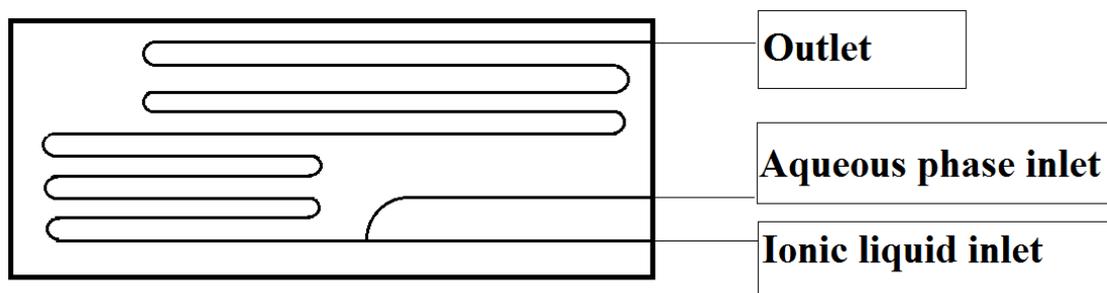
Fig. 2. Top view sketch of the 0.2mm ID microchip.
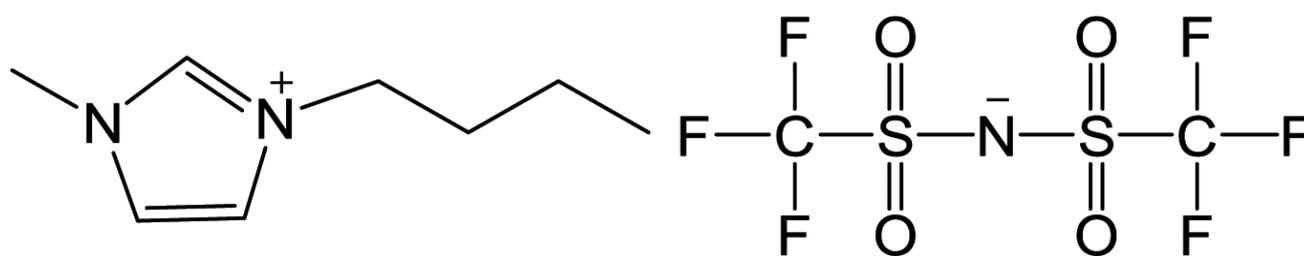
Fig. 3. Chemical structure of the ionic liquid 1-butyl-3-methylimidazolium

bis[(trifluoromethyl)sulfonyl]amide ([C$_4$min][NTf$_2$]).
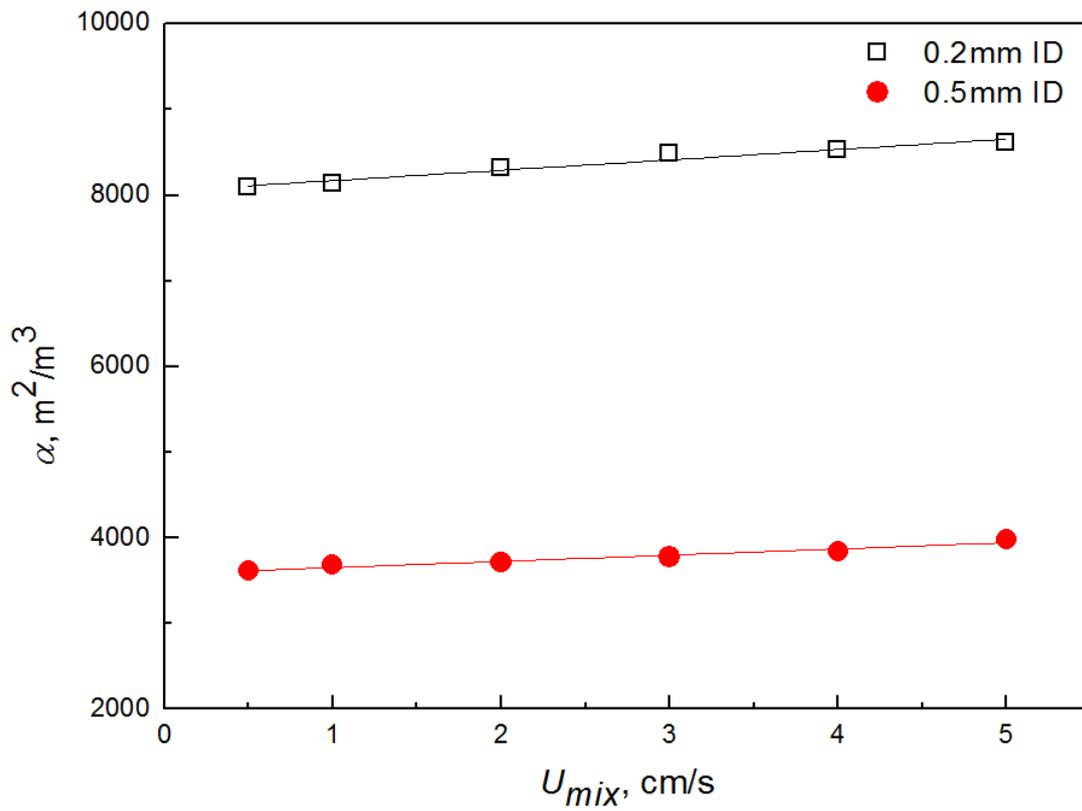
Fig. 4. Specific interfacial area against mixture velocity for different capillary diameters
Aqueous phase: 1M nitric acid; organic phase: 0.2M CMPO-1.2M TBP/[C4mim][NTf$_2$].
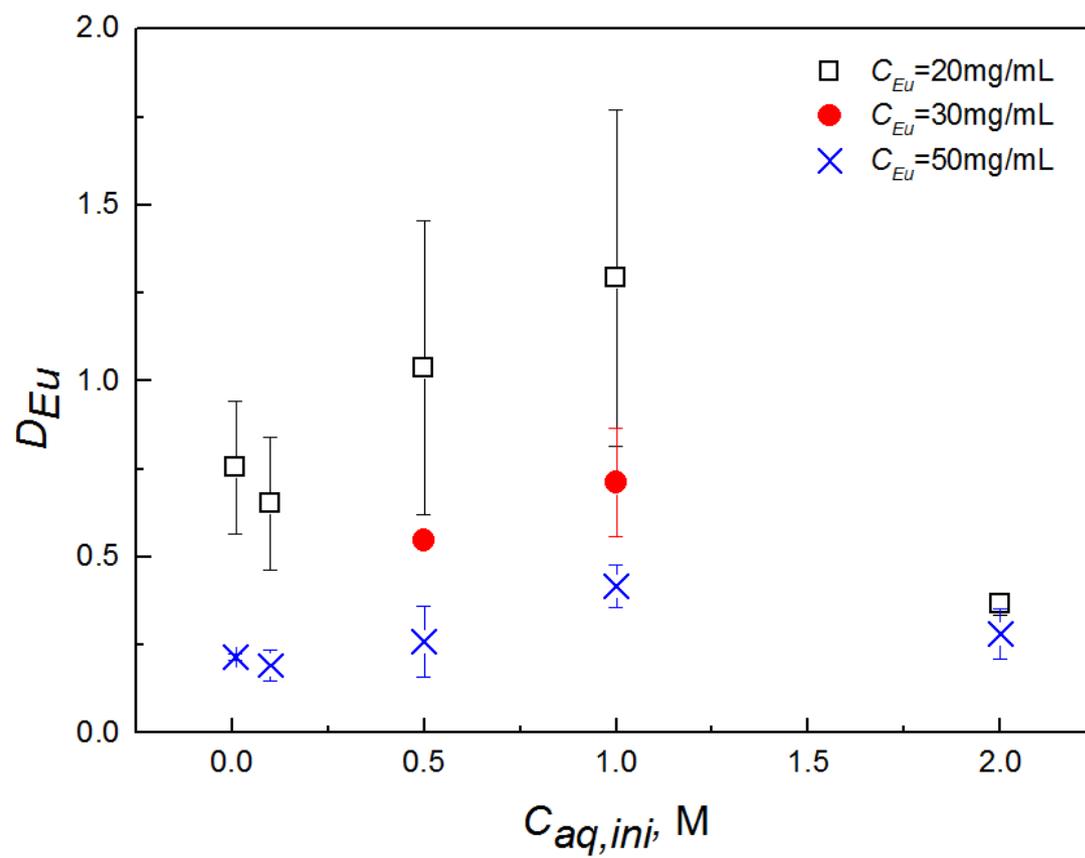
Fig. 5. Eu(III) distribution coefficients against initial nitric acid concentration at different initial Eu(III) loading. Aqueous phase: 0.01-2M HNO3; organic phase: 0.2M CMPO-1.2M TBP/[C4mim][NTf2].
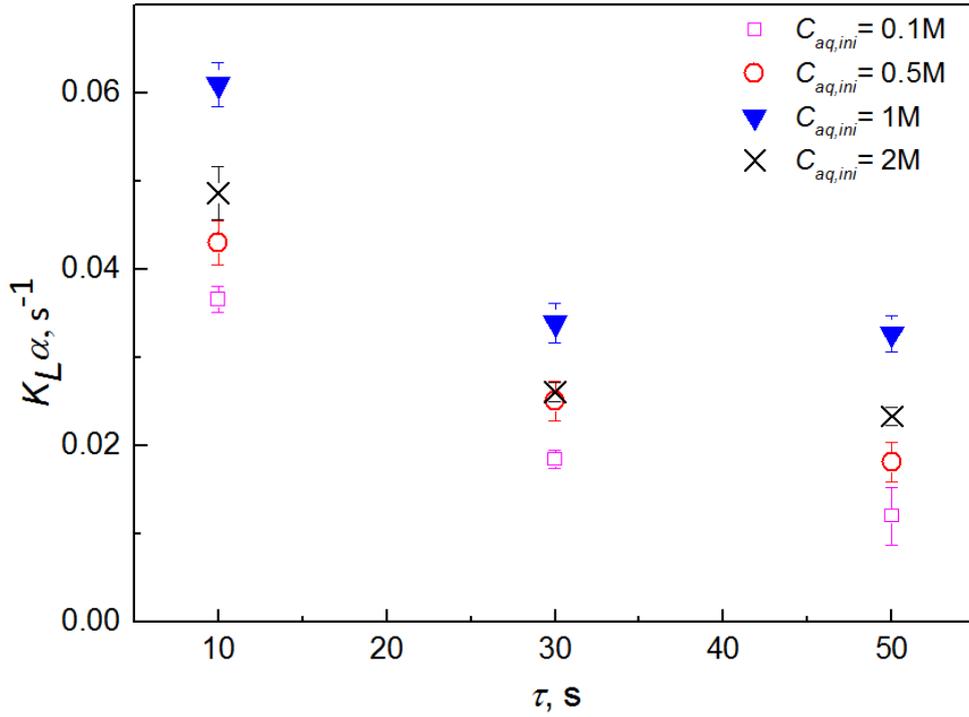
(a) Volumetric mass transfer coefficients
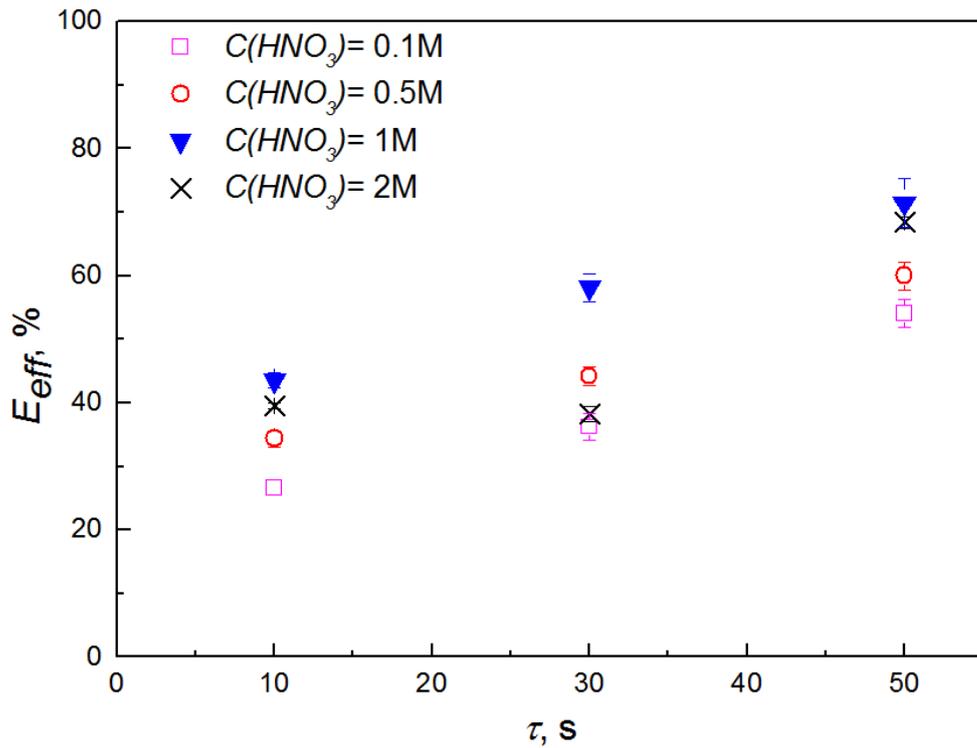
(b) Extraction efficiency

Fig. 6. Variation of Eu(III) (a) extraction efficiency and (b) volumetric mass transfer coefficient with residence time for different initial nitric acid concentrations; U_{mix}=0.5cm/s, CL=5, 15, 25cm.
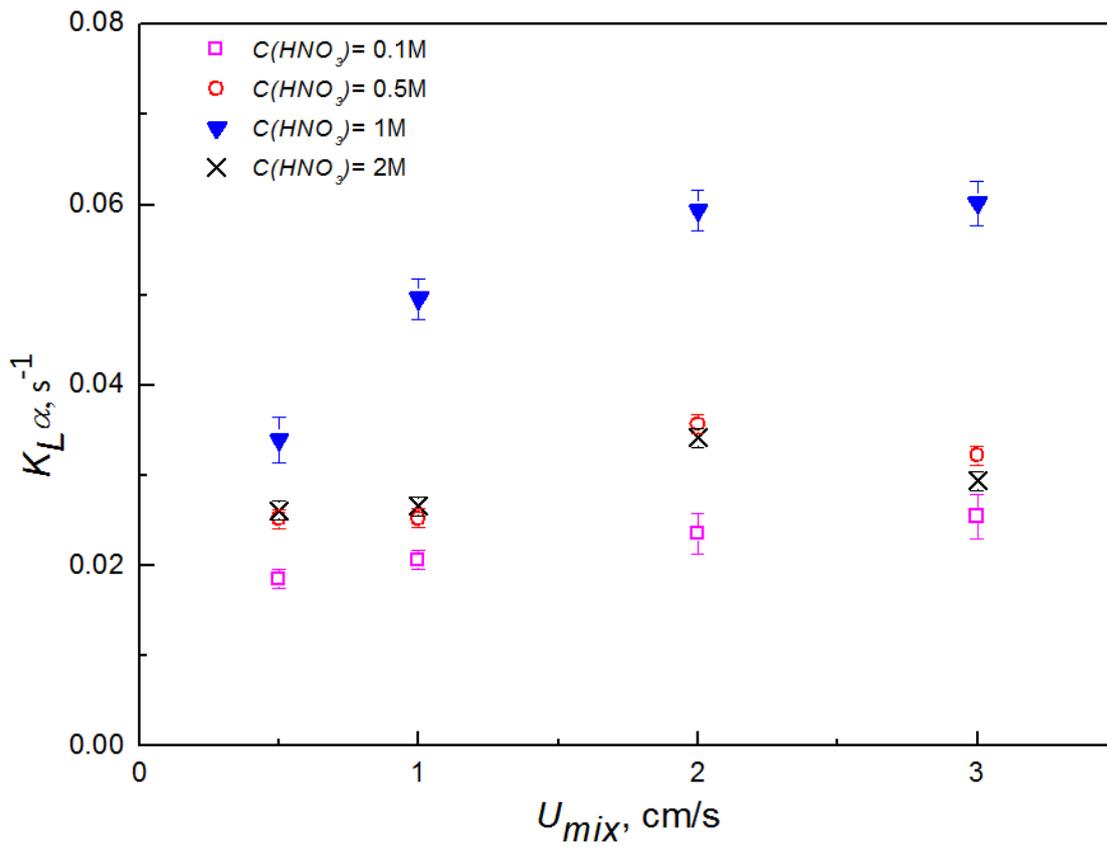
Fig. 7. Variation of Eu(III) volumetric mass transfer coefficient with mixture velocity for different initial nitric acid concentrations; CL=15cm, 0.5mm ID.
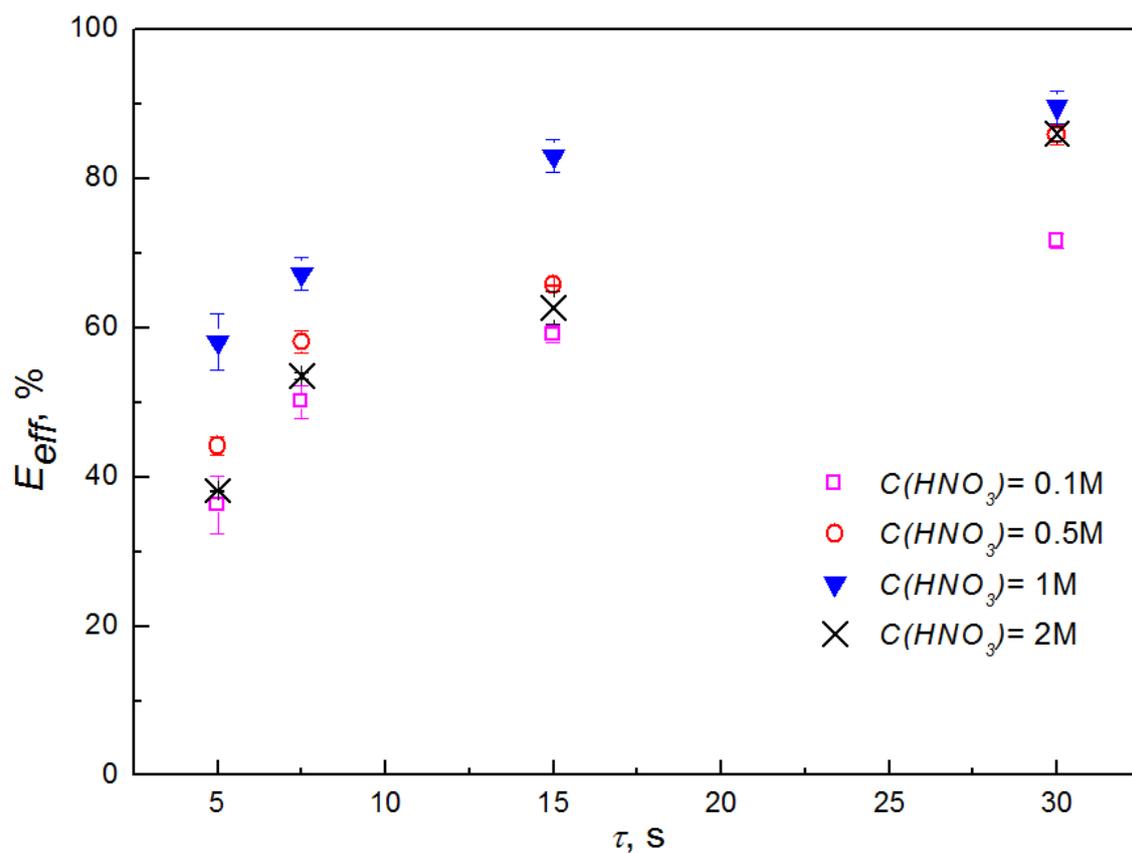
Fig. 8. Variation of Eu(III) extraction efficiency with residence time for different initial nitric acid concentrations; *CL*=15cm, 0.5mm ID.
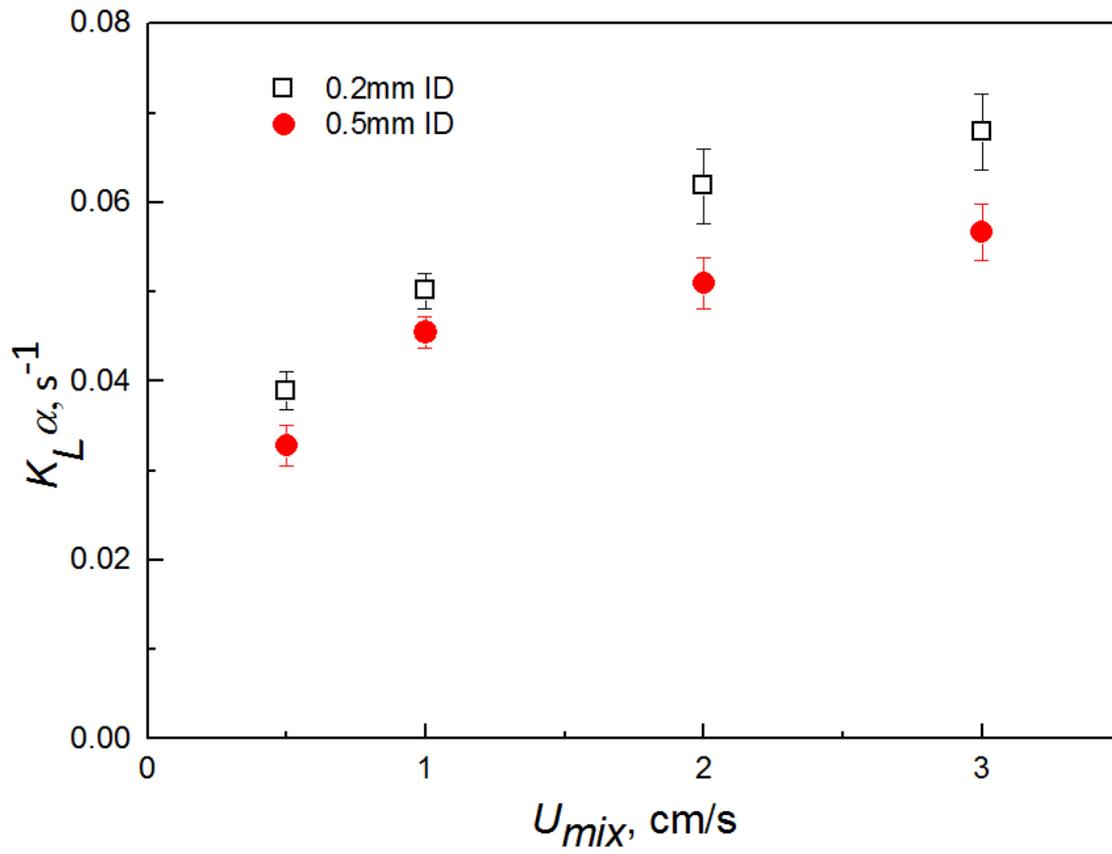
Fig. 9. Variation of Eu(III) volumetric mass transfer coefficient with mixture velocity for different capillary sizes, 0.2mm and 0.5mm ID; *CL*=25cm.

(a) Averaged recirculation pattern

τ_{min}=0.523s
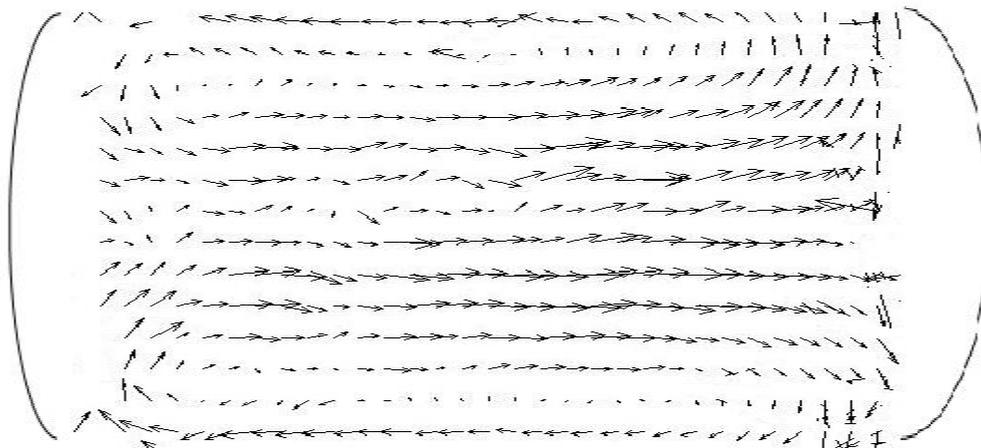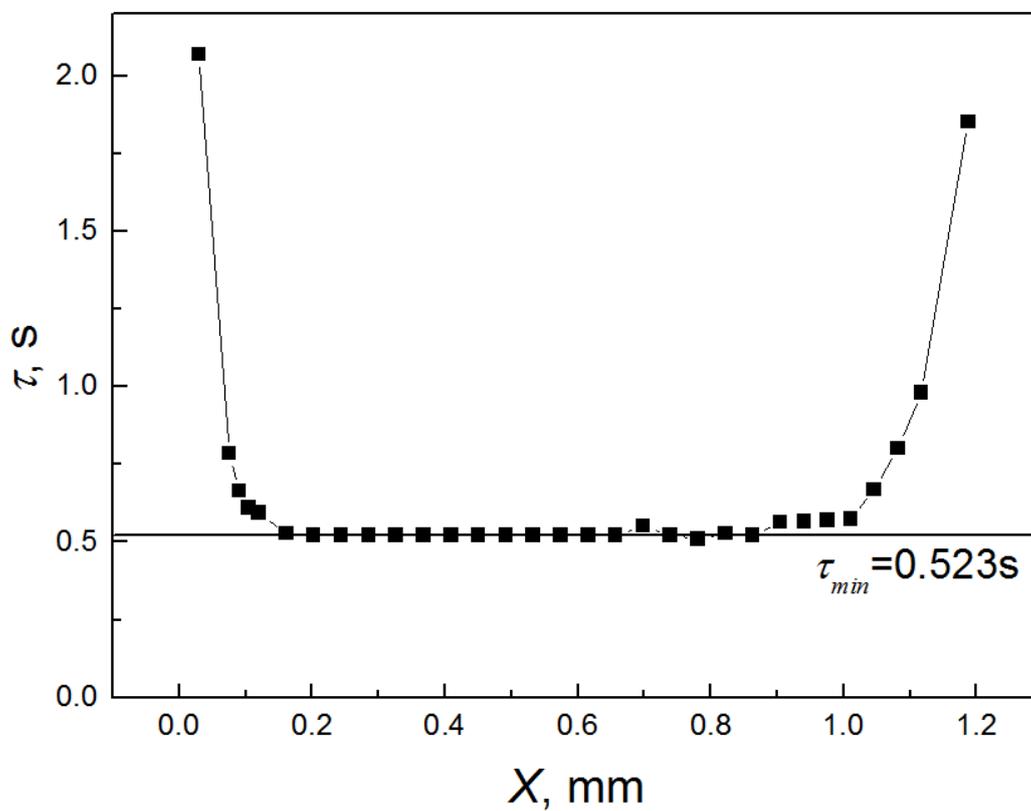
(b) Averaged recirculation time

Fig.10. (a) Averaged recirculation pattern and (b) averaged recirculation time profile along an aqueous plug; 0.5mm ID channel, $Q_{aq}=Q_{IL}$=3.534ml/h
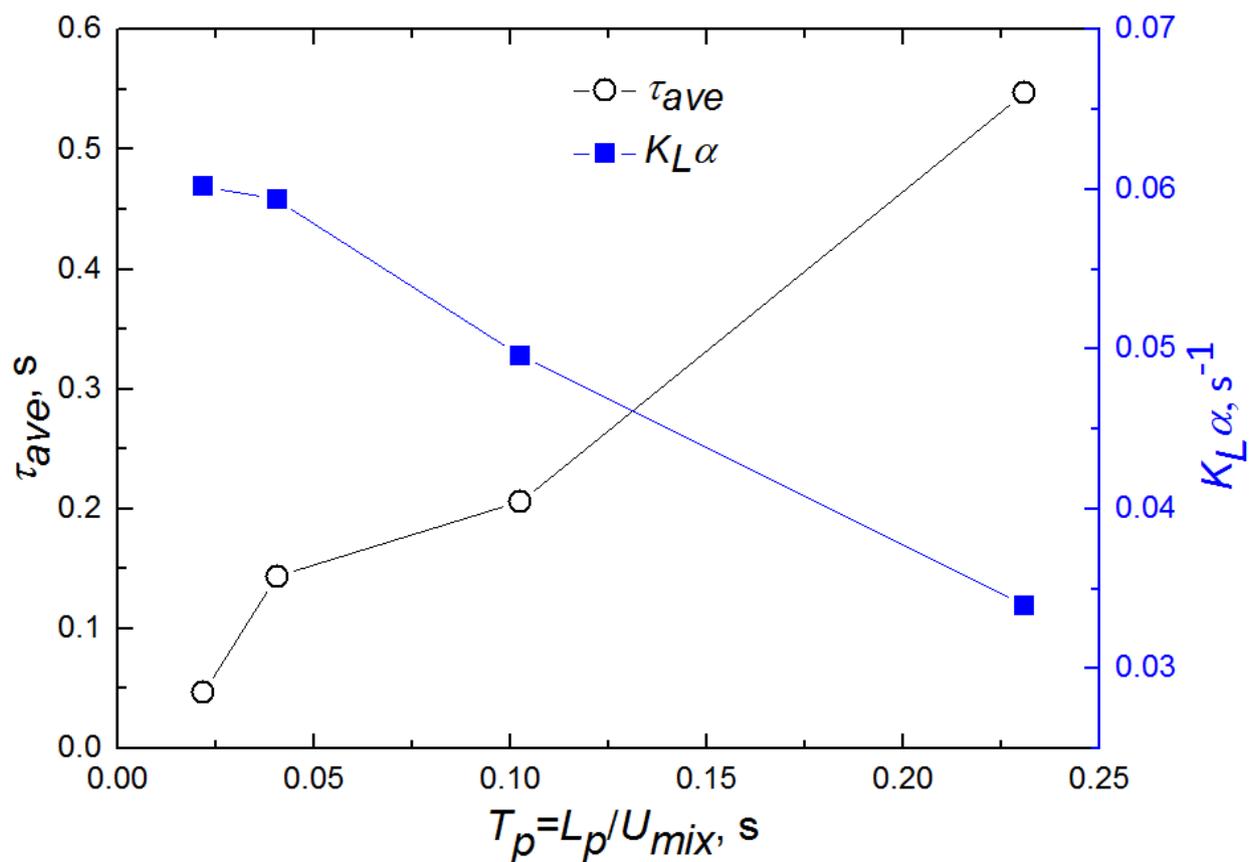
Fig. 11. Recirculation time and mass transfer coefficient as a function of plug travel time
Aqueous phase: 1M nitric acid; organic phase: 0.2M CMPO-1.2M TBP/[C$_4$mim][NTf$_2$]; CL=15cm;
0.5mm ID; Q_{aq}=Q_{IL}
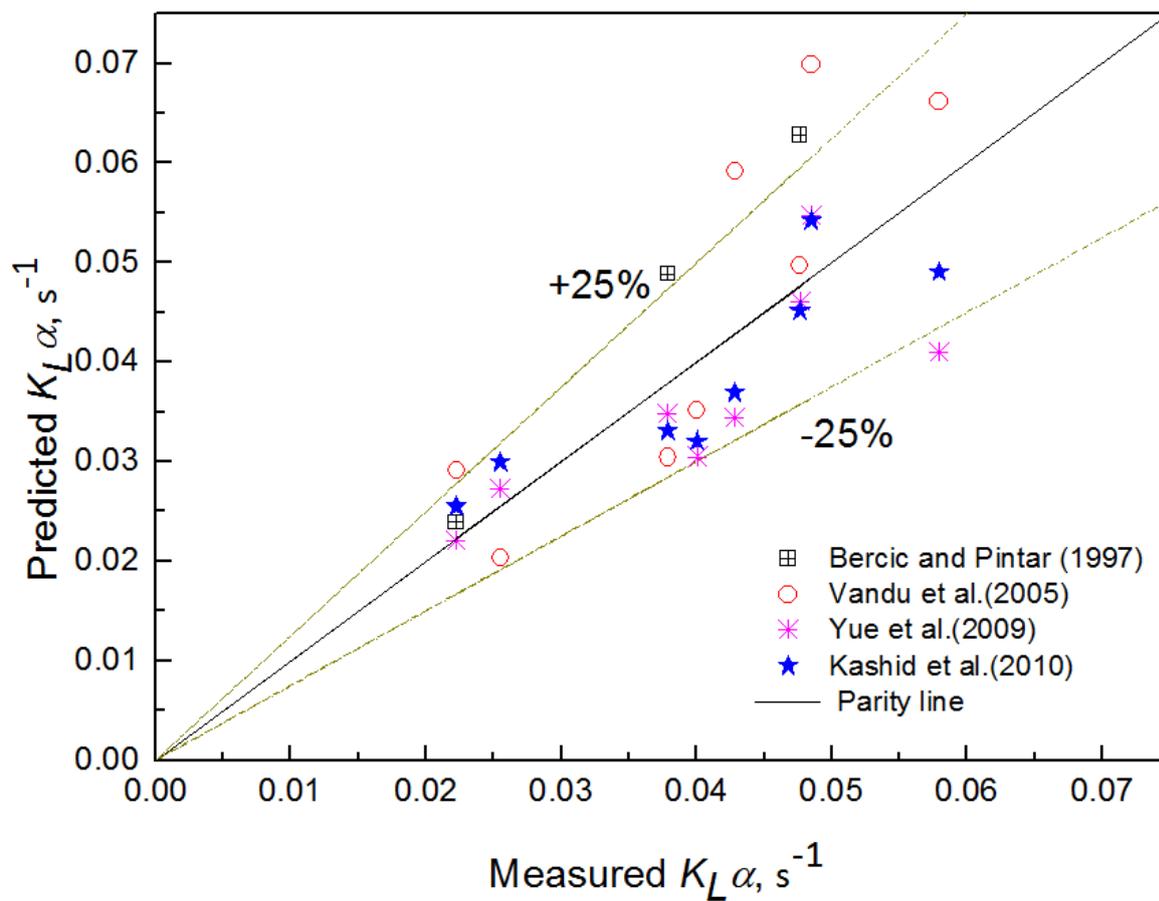
Fig. 12. Comparison of experimental K_La values against predicted ones.
(System: 1M nitric acid-0.2M CMPO-1.2M TBP/[C$_4$mim][NTf$_2$]; $Q_{aq}=Q_{IL}$; ID=0.2 and 0.5 mm capillary)